

Particle Accelerators in the Hot Spots of Radio Galaxy 3C 445, Imaged with the VLT

M. Almudena Prieto,^{1*} Gianfranco Brunetti,² Karl-Heinz Mack^{2,3}

Hot spots (HSs) are regions of enhanced radio emission produced by supersonic jets at the tip of the radio lobes of powerful radio sources. Obtained with the Very Large Telescope (VLT), images of the HSs in the radio galaxy 3C 445 show bright knots embedded in diffuse optical emission distributed along the post-shock region created by the impact of the jet into the intergalactic medium. The observations reported here confirm that relativistic electrons are accelerated by Fermi-I acceleration processes in HSs. Furthermore, both the diffuse emission tracing the rims of the front shock and the multiple knots demonstrate the presence of additional continuous re-acceleration processes of electrons (Fermi-II).

HSs are common features in powerful extragalactic lobe-dominated radio sources (Fanaroff-Riley class II). Their radio spectra are interpreted in terms of synchrotron radiation. Detection of optical radiation from HSs is difficult due to the natural decay of the synchrotron spectrum toward higher frequencies. Yet, the optical detection of HSs has a number of fundamental implications in our understanding of the physics of particle acceleration in these regions. Relativistic electrons rapidly lose their energy emitting synchrotron radiation, and the radiative lifetime of the electrons responsible for the emission in the optical band is ~ 300 times shorter—between a few hundred and a few thousand years, depending on the magnetic field strength—than that of the less energetic electrons emitting in radio wavelengths. As a consequence, optical detection of HSs implies either an extremely efficient transport of the ultra-relativistic particles from the core to the HS (1) or the in situ production of such energetic particles with Lorentz factors $\gamma > 10^5$ to 10^6 , where the Lorentz factor γ is defined as $\gamma = (1 - [(v)/(c)]^2)^{-1/2}$ (2). Although the search for optical emission from radio HSs has a long history (3–5), few HSs have been detected as synchrotron emitters at optical frequencies (6). Indeed, at high frequencies most well-studied HSs show an abrupt steepening of the spectrum below the straight power law extrapolated from the low frequencies, which is interpreted as a result of a high-energy cutoff in the spectrum of the synchrotron-emitting electrons. Thus far, there are only two known HSs in

which the radio power law spectrum can be extrapolated up to the optical or ultraviolet regime (3C 303) (7) or even to the x-ray regime (3C 390.3) (8), indicating the continuation of the synchrotron emission to higher energies. In the case of optical detection, the short radiative lifetime of the emitting electrons as well as their diffusion-length scale of much less than 1 kpc make high-resolution optical imaging (so far obtained only with Hubble Space Telescope) (9) an unequaled tool with which to sample those regions where high-energy electrons are injected and/or re-accelerated.

Here, we report on the imaging of the local accelerator regions in the southern HS of the radio galaxy 3C 445. 3C 445 is a classical double-lobe radio source at redshift $z = 0.0562$. At the tips of each lobe are the southern HS, placed at ~ 450 kpc (the Hubble constant, $H_0 = 50 \text{ km s}^{-1} \text{ Mpc}^{-1}$; the deceleration parameter, $q_0 = 0.5$), and the northern HS at a projected distance of ~ 460 kpc from the core (10). Both HSs were observed with the Very Large Telescope (VLT) of the European Southern Observatory and the Infrared Spectrometer and Array Camera, at the bands K_s (2.2 μm), H (1.7 μm), and J_s (1.2 μm), and the Focal Reducer–low-dispersion spectrograph at the I-band (0.9 μm). Each final image is the result of stacking between 10 (I band) and 30 to 40 (J_s , H, and K_s band) slightly shifted frames. Sky background removal was done by a median filter of several adjacent frames. The integration time ranged from 35 to 60 min, depending on the band. The final image quality has an equivalent full width at half maximum of 0.6 arc sec in K_s , 0.5 arc sec in H, 0.45 arc sec in J_s , and 0.55 arc sec in I. The counterpart of the radio emission from each HS was detected in all bands. The emission is extended in both cases and in all filters, but only the emission in the southern HS could be resolved in several compact regions. Thus, we focus our analysis and discussion on the southern HS.

The emission from the southern HS of 3C 445 is resolved in at least three compact regions (Fig. 1). These regions are further enclosed by diffuse emission detected at about the 5σ level in all bands; the diffuse emission is more evident in the lower-frequency images. The overall optical and infrared emission has an arc-like shape and size as in the radio image, presenting the typical structure of a post-shock region usually seen at radio waves (10). We checked whether the electrons responsible for the synchrotron emission could have been transported by the jet from the core of the galaxy to the HS. The maximum distance electrons can travel away from the galaxy nucleus depends on their synchrotron and inverse Compton (IC) radiative lifetimes ($\propto 1/\gamma$) as well as on the velocity of the jet. The Lorentz factor of the electrons emitting synchrotron radiation in the I band is $\gamma \sim 3 \times 10^6 B^{-1/2}$, where B is the magnetic field strength in the HS region in nT. A first estimate of B can be derived assuming the usual equipartition conditions (11): From the observed synchrotron luminosity (Fig. 2) and the radio HS size (4.8×2 arc sec), $B \cong 2.8$ nT and the corresponding Lorentz factor is thus $\gamma \sim 2 \times 10^6$.

The maximum distance (projected on the plane of the sky) the optical electrons in 3C 445 South could have reached away from the nucleus of the galaxy is less than 100 kpc, independent of the jet velocity and assuming that the electrons suffer only IC losses due to the interaction with the microwave photons [i.e., the intrinsic magnetic field is neglected (12)]. Yet, HS 3C 445 South is 450 kpc from the core and, thus, the optical electrons witnessed must be produced in place.

An effective mechanism to accelerate relativistic electrons in the HSs of radio galaxies to the required energies, $\gamma \sim 10^5$ to 10^6 , to emit optical light, is strong shocks. Strong shocks are expected to be produced by the impact of the jet into the intergalactic medium (6, 13). From an observational point of view, the bow-shock shape seen in the images of the southern HS in 3C 445 at the tip of the radio lobe supports the shock-wave scenario. The integrated magnitudes in the K_s (18.5 ± 0.09), H (19.5 ± 0.2), J_s (20.3 ± 0.1), and I (21.3 ± 0.1) bands of the HS, together with the integrated emission at 8.4 GHz [90 ± 9 mJy, where $1 \text{ Jy} = 10^{-26} \text{ W m}^{-2} \text{ Hz}^{-1}$], were fit to theoretical synchrotron spectra produced by a population of accelerated electrons [after (14)]. Assuming a power law electron distribution with typical injection spectral indices $\delta = 2.0$ to 2.2, the models can successfully reproduce the data with a best-fit cutoff frequency (ν_c , the synchrotron frequency emitted by the electrons accelerated at the maximum energy), $\nu_c \sim 1$ to 2×10^{15} Hz (Fig. 2). For those parameters, the break of the synchrotron spectrum (ν_b , the synchrotron frequency emitted by electrons of Lorentz factor γ_b ; beyond that, radiative losses cause a steepening of

¹European Southern Observatory, Karl-Schwarzschild-Str. 2, D-85748 Garching, Germany. ²Istituto di Radioastronomia del CNR, Via P. Gobetti 101, I-40129 Bologna, Italy. ³ASTRON/NFRA, Postbus 2, NL-7990 AA Dwingeloo, Netherlands, and Radioastronomisches Institut der Universität Bonn, Auf dem Hügel 71, D-53121 Bonn, Germany.

*To whom correspondence should be addressed. E-mail: aprieto@eso.org

REPORTS

the electron spectrum) occurs at $v_e/v_b \cong 300 \pm 100$ for $\delta = 2.2$, and at $v_e/v_b \cong 1000 \pm 300$ for $\delta = 2.0$ (errors at 90% confidence level). Because there are no radio observations with sufficiently high resolution, attempts to determine individual synchrotron spectra for the brightest compact regions in the HS are currently inconclusive; however, $v_e > 3 \times 10^{14}$ Hz is obtained for the three main knots in the HS.

Numerical simulations of HSs (15–18) show that a high-pressure cap is formed at the tip of the jet, from where the pressured plasma escapes backward into a larger, diffuse region, or cocoon, that forms around the jet. The VLT observations show a “primary” knot, identified as the tip of the jet characterized by its enhanced brightness; two “secondary” fainter knots, on each side of the primary; and diffuse emission with a bow-shock shape that we associate with the emission from the plasma which escapes from the shock region into the cocoon. However, the detection of emission up to 3 to 5 kpc away from the primary knot is surprising because, assuming an equipartition magnetic field in the HS, the optical-emitting electrons have a radiative lifetime of $\sim 2 \times 10^4$ years and thus a typical travel length $\ll 1$ kpc. Consequently, unless an improbably low intrinsic magnetic field $B < 0.5$ nT is assumed, optical and infrared emission on scales larger than 1 kpc provides direct evidence for additional in situ re-acceleration in the HS region with an acceleration time scale of the order of 10^4 year. Similar evidence has recently been observed in extragalactic optical jets (e.g., 3C 273) (19).

In addition, the appearance of multiple knots may indicate the presence of incipient Rayleigh-Taylor instabilities that produce variations in the plasma density and path length, leading to multiple emitting components such as those expected by simulated synchrotron images of HSs (18, 20). The development of Rayleigh-Taylor instabilities in the cocoon may power magnetohydrodynamic (MHD) turbulence that can account for the required additional re-acceleration of the relativistic electrons downstream.

Assuming Alfvénic turbulence in the cocoon, the MHD Fermi-II-like acceleration time [(21) and references therein] is

$$\tau_{acc}^{II}(\text{sec}) \sim \frac{l c}{v_A^2} \left(\frac{\delta B}{B} \right)^{-2} \quad (1)$$

where l is the typical distance between the peaks of turbulence responsible for Fermi-II acceleration, v_A is the Alfvén velocity, and c is the speed of light. In following with Eq. 1, the acceleration efficiency ($1/\tau$) is proportional to the energy density in turbulence waves with scales $< l$, defined as $(\delta B)^2/8\pi$. The scale l should be between the minimum scale ($\sim 2\pi v_i/\Omega_i$, with v_i and Ω_i as the sound velocity and the cyclotron frequency of the ions, respectively) and the maximum scale of the turbulence in the plasma. Two regimes of plasma

temperatures are considered. For $T < 10^7$ K, the largest possible scale of the undamped Alfvénic turbulence is $l_{max} = 2\pi/k_{min}$, where

$k_{min} \sim (\epsilon/v_D^3)^{1/4} \text{ m}^{-1}$ [(22) and references therein]. The dissipation coefficient v_D relevant for the damping of the turbulence waves

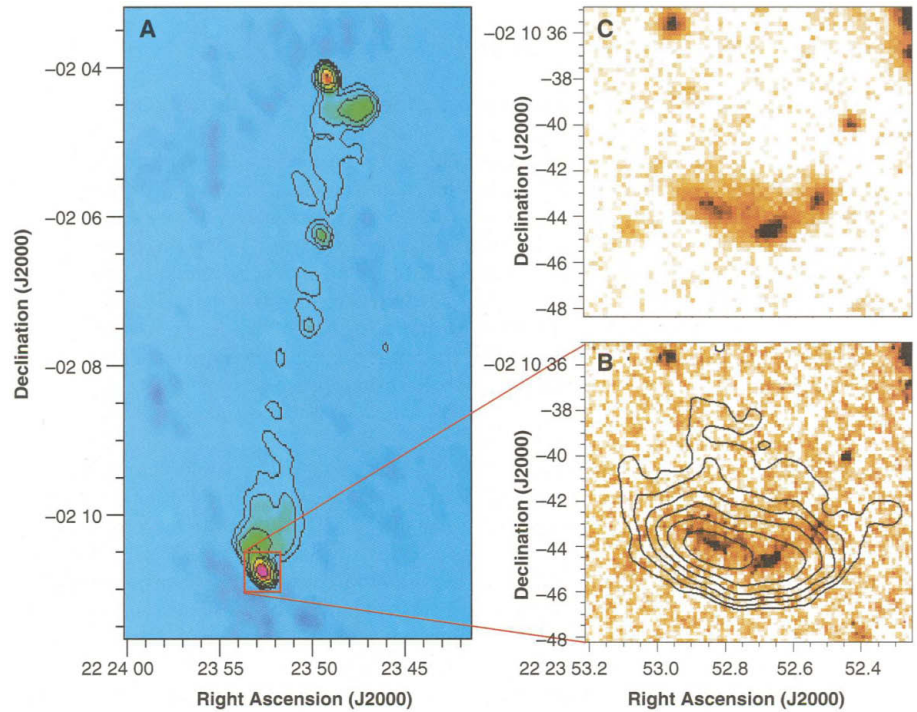
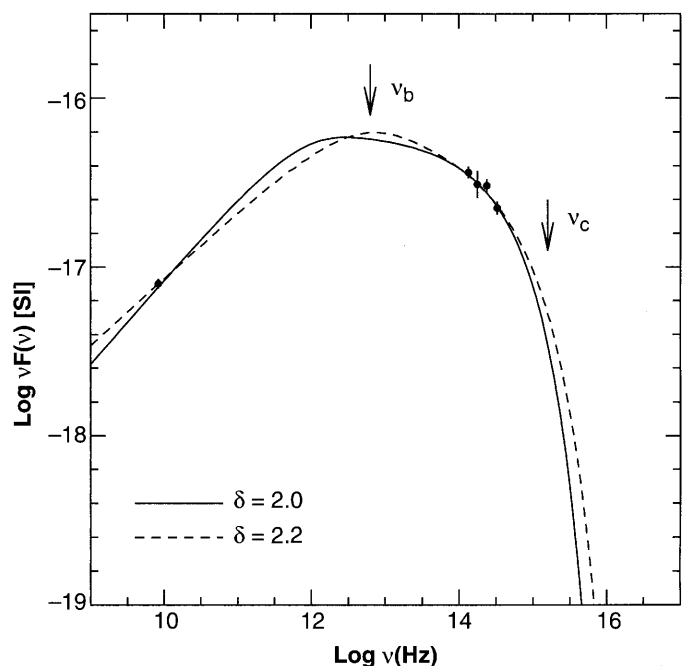


Fig. 1. (A) Radio contours and colors from a snapshot observation of 3C 445 obtained with the Very Large Array (VLA) in D-configuration at 8.4 GHz; contour levels are 2, 4, 8, 16, 32, 64 mJy/beam. Color wedge scales from 0.5 mJy per beam (blue, background noise level) to 100 mJy per beam (red, peak flux density). (B) Enlarged image of the southern HS region observed at the same frequency with the VLA B array; the half-power beam width is 1.1 arc sec. The radio contours show the southernmost part of the HS and are superimposed on the VLT J_s image (23). The radio maps were reduced from data requested from the National Radio Astronomy Observatory VLA archive; contour levels are 0.25, 0.5, 1, 2, 4, 8 mJy/beam; color wedge scales linearly from ~ 23.8 (darkest emission), 25.4 (diffuse emission), to 25.5 (background) mag/beam. (C) The VLT I band image of the southern HS region; color wedge ranges from ~ 24.5 (darkest), 26.2 (diffuse), to 27 (background) mag/beam.

Fig. 2. Best synchrotron model fits to HS 3C 445 South. The solid circles denote the energies as obtained from the radio data (8.4 GHz) and the infrared and optical measurements (K, H, J, and I band). The models correspond to an injection spectral index of the electron distribution $\delta = 2.0$ or 2.2. The best-fit cutoff and break frequencies are $\nu_c = 1.0 \times 10^{15}$ Hz and $\nu_b = 1.0 \times 10^{12}$ Hz ($\delta = 2.0$) or $\nu_c = 1.8 \times 10^{15}$ Hz and $\nu_b = 5.9 \times 10^{12}$ Hz ($\delta = 2.2$), respectively. The positions of the best-fit cutoff and break frequencies in the case of $\delta = 2.2$ are indicated by the arrows.



REPORTS

is $v_D \sim 3.8 \times 10^{10} T^{5/2}/n_p$, whereas ϵ ($\text{J kg}^{-1} \text{s}^{-1}$) is the energy source of the fluctuations that balances the dissipation. For proton thermal densities $n_p \sim 10^2 \text{ m}^{-3}$ assuming $\epsilon \sim 0.1 \text{ J kg}^{-1} \text{ s}^{-1}$ typical of HSs (22), the maximum scale of the turbulence is found $l_{\text{max}} \sim 20(T/5 \times 10^5)^{15/8} \text{ pc}$. Substituting this value in Eq. 1 with $\delta B/B \sim 1$ and $v_A \sim 5 \times 10^6 \text{ m s}^{-1}$, the Fermi-II-like acceleration time is

$$\tau_{\text{acc}}^{\text{II}} \sim 2 \times 10^5 (l/l_{\text{max}})(T/5 \times 10^5)^{15/8} \text{ year} \quad (2)$$

As a consequence, waves with turbulence scales of $\sim 0.1 \times l_{\text{max}}$ (which account for the bulk of the energy) can easily power Fermi-II processes. For $T > 10^7 \text{ K}$, which is typical of the intra-cluster medium, damping processes are less efficient and the largest turbulence scale is limited by the injection scale: here, of the order of the transverse dimension of the downstream region, i.e., $l_{\text{max}} \sim 1 \text{ kpc}$. Assuming $\delta B_k^2 \propto k^{-s}$ ($\delta B_k^2/8\pi$ is the differential energy density in waves between k and $k + dk$ and $s = 5/3$ in the Kolmogorov case, $s = 3/2$ in the Kraichnan case) and $\delta B^2 = \int dk \delta B_k^2 \sim B^2$, we find that in the Kraichnan case, $\tau_{\text{acc}}^{\text{II}} \sim 3$ to $6 \times 10^4 \text{ year}$ for $l \sim 0.1$ to 0.2 pc . Waves with that turbulence scale contain enough energy density to accelerate the optical-emitting electrons. However, in the Kolmogorov case MHD Fermi-II-like acceleration is less efficient and very strong turbulence, $\delta B/B \sim 2$ to 5 , is required.

To test whether additional Fermi-II-like acceleration in the downstream region can account for the observed properties of the observed HS, a calculation of the plasma

evolution in three phases was considered. This calculation attempts to mimic the behavior of the plasma in HSs as seen in MHD simulations. First, the relativistic electrons diffuse, expanding from the high-pressure region (central primary knot), being also subjected to synchrotron and IC losses. Second, an approximate pressure balance is reached and electrons suffer only synchrotron and IC losses. Finally, the plasma is recompressed in the regions of the two secondary knots, possibly due to the development of nonlinear plasma instabilities. During the three phases, relatively efficient ($\tau_{\text{acc}}^{\text{II}} \sim 2$ to $5 \times 10^4 \text{ year}$) second-order Fermi re-acceleration mechanisms are assumed. We calculated the evolution of the electron energy considering a magnetic field frozen into the plasma (homogeneous) and obtained the synchrotron cutoff frequency, ν_c , as a function of the distance from the primary knot for different model parameters (Fig. 3). Assuming a canonical transport velocity from the primary knot in the range 0.03 to $0.1 c$, we found that the combined effect of adiabatic expansion (during the first phase) and second-order Fermi processes can maintain ν_c high enough to have optical and infrared emission from secondary knots located at $\sim 3 \text{ kpc}$ distance from the primary knot and still have detectable residual extended optical and infrared emission in between the knots. More specifically, we find that this scenario works only if we assume relatively strong expansion factors during the first phase ($f > 2$, where f is

defined as the ratio between the size of the plasma region after and before the compression or expansion) to alleviate the strong synchrotron losses in the region of the primary knot, and if we assume a relatively low initial magnetic field strength $B \leq 15 \text{ nT}$ (at least for a conservative $f > 0.25$ during the third phase). We also found that such a limit yields a magnetic field strength averaged over the total HS region $\leq 4 \text{ nT}$, which is consistent with the field strength estimated from equipartition. The above limit on the magnetic field strength and the derived ν_c from the synchrotron spectrum allow constraining the efficiency of the acceleration in the primary knot, where the relativistic electrons are accelerated directly by the shock (Fermi-I). The acceleration efficiency here is higher: $\tau_{\text{acc}}^{\text{I}} \sim 10^3 (B/15)^{-3/2} \text{ year}$, as expected.

References and Notes

1. W. Kundt, Gopal-Krishna, *Nature* **288**, 149 (1980).
2. K. Meisenheimer *et al.*, *Astron. Astrophys.* **219**, 63 (1989).
3. W. C. Saslaw, J. A. Tyson, P. Crane, *Astrophys. J.* **222**, 435 (1978).
4. S. M. Simkin, *Astrophys. J. Lett.* **222**, 55 (1978).
5. P. Crane, J. A. Tyson, W. C. Saslaw, *Astrophys. J.* **265**, 681 (1983).
6. K. Meisenheimer, M. G. Yates, H.-J. Röser, *Astron. Astrophys.* **325**, 57 (1997).
7. W. C. Keel, *Astrophys. J.* **329**, 532 (1988).
8. M. A. Prieto, *Mon. Not. R. Astron. Soc.* **284**, 627 (1997).
9. R. C. Thomson, P. Crane, C. Mackay, *Astrophys. J. Lett.* **446**, 93 (1995).
10. J. P. Leahy *et al.*, *Mon. Not. R. Astron. Soc.* **291**, 20 (1997).
11. A. G. Pacholczyk, *Radio Astrophysics* (Freeman, San Francisco, 1970).
12. Gopal-Krishna, P. Subramanian, P. J. Wiita, P. A. Becker, *Astron. Astrophys.* **377**, 827 (2001).
13. G. Brunetti *et al.*, *Astrophys. J. Lett.* **561**, 157 (2001).
14. G. Brunetti, M. Bondi, A. Comastri, G. Setti, *Astron. Astrophys.* **381**, 795 (2002).
15. M. L. Norman, K.-H. A. Winkler, L. Smarr, M. D. Smith, *Astron. Astrophys.* **113**, 285 (1982).
16. S. Massaglia, G. Bodo, A. Ferrari, *Astron. Astrophys.* **307**, 997 (1996).
17. J. M. Martí, E. Müller, J. A. Font, J. M. Ibanez, A. Marquina, *Astrophys. J.* **479**, 151 (1997).
18. M.-A. Aloy, J.-L. Gomez, J.-M. Ibanez, J.-M. Martí, E. Müller, *Astrophys. J. Lett.* **528**, 85 (2000).
19. S. Jester, H.-J. Röser, K. Meisenheimer, R. Perley, R. Conway, *Astron. Astrophys.* **373**, 447 (2001).
20. M. D. Smith, M. L. Norman, K.-H. A. Winkler, L. Smarr, *Mon. Not. R. Astron. Soc.* **214**, 67 (1985).
21. M. Gitti, G. Brunetti, G. Setti, *Astron. Astrophys.* **386**, 456 (2002).
22. C. Lacombe, *Astron. Astrophys.* **54**, 1 (1977).
23. The positional coincidence between optical, infrared, and radio data has been very carefully checked using the galaxy core position (for the radio maps) and the position of nearby stars taken from the USNO-A2.0 catalog (for the optical maps, accuracy = 0.25 arc sec).
24. K.-H.M. was supported by a Marie Curie Fellowship of the European Commission. G.B. acknowledges partial financial support from the Italian MIUR (Ministero dell'Istruzione dell'Università e della Ricerca) under grant Cofin01-02-8773. We would like to thank the staff at the VLT Paranal Observatory for their professional service. We are grateful to M. Bondi, I. M. Gioia, M. J. M. Marchà, K. Meisenheimer, M.-A. Pérez-Torres, G. Setti, and S. R. Spangler for their valuable comments on the manuscript.

10 July 2002; accepted 4 September 2002

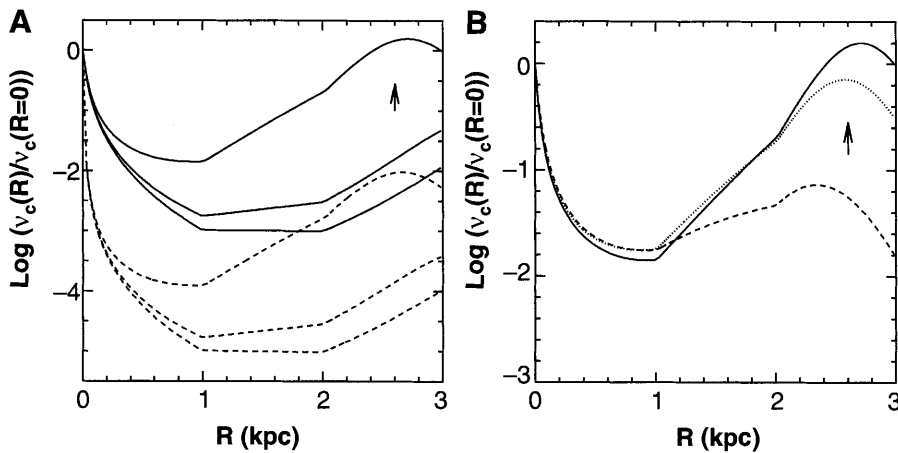


Fig. 3. The calculated cutoff frequency, ν_c , of the synchrotron spectrum (relative to the value at the "primary" knot) is plotted as a function of the distance R from the primary knot ($R = 0$); the farthest "secondary" knot is at $R = 3 \text{ kpc}$. The arrows give the limits of ν_c for the stronger secondary knot. The calculations do not take into account the finite resolution obtained in the VLT images (Fig. 1; spatial resolution $\sim 0.7 \text{ kpc}$) and the projection effects. The lengths and durations in the three-phase calculation are assumed to be similar and are adjusted to $l = 1 \text{ kpc}$ to match the observed distribution of the knots. (A) Model calculations for an expansion factor $f = 3$ during the first phase (0 to 1 kpc) and a compression factor $f = 0.5$ during the third phase (2 to 3 kpc), assuming as initial magnetic field strengths $B = 8 \text{ nT}$ (solid lines) and $B = 30 \text{ nT}$ (dashed lines). From the bottom to the top of the diagram, for each value of B , the Fermi-II acceleration time is $\tau_{\text{acc}}^{\text{II}} = 10^8, 10^5$, and $2 \times 10^4 \text{ year}$, respectively. (B) Model calculations for an initial magnetic field strength $B = 8 \text{ nT}$, for a Fermi-II acceleration time $\tau_{\text{acc}}^{\text{II}} = 2 \times 10^4 \text{ year}$ and for a compression factor $f = 0.5$ during the third phase (2 to 3 kpc). Different lines correspond to different expansion factors during the first phase (0 to 1 kpc): $f = 3$ (solid line), $f = 2.5$ (dotted line), and $f = 1.5$ (dashed line).